Nonequilibrium Lattice Dynamics in Monolayer MoS₂

Fabio Caruso*

Institut für Theoretische Physik und Astrophysik, Christian-Albrechts-Universität zu Kiel, Kiel, Germany

E-mail: caruso@physik.uni-kiel.de

Abstract

The coupled nonequilibrium dynamics of electrons and phonons in monolayer MoS₂ is investigated by combining first-principles calculations of the electron-phonon and phononphonon interaction with the time-dependent Boltzmann equation. Strict phase-space constraints in the electron-phonon scattering are found to influence profoundly the decay path of excited electrons and holes, restricting the emission of phonons to crystal momenta close to few high-symmetry points in the Brillouin zone. As a result of momentum selectivity in the phonon emission, the nonequilibrium lattice dynamics is characterized by the emergence of a highlyanisotropic population of phonons in reciprocal space, which persists for up to 10 ps until thermal equilibrium is restored by phonon-phonon scattering. Achieving control of the nonequilibrium dynamics of the lattice may provide unexplored opportunities to selectively enhance the phonon population of two-dimensional crystals and, thereby, transiently tailor electron-phonon interactions over sub-picosecond time scales.

Transition-metal dichalcogenides (TMDs) exhibit strong light-matter coupling, ¹ a rich photo-physics, ² and a unique interplay of spin, ^{3,4} valley, ^{5,6} lattice, ⁷ and electronic ⁸ degrees of freedom. These characteristics, along-side with numerous possibilities to tailor screening, ⁹ charge-carrier density, ⁷ and dimensionality, ^{10,11} make them promising candidates for the exploration of new pathways to achieve

properties on demand in quantum matter. 12 A broad spectrum of emergent phenomena can indeed be realized and controlled in these compounds via coupling to femtosecond light pulses, including phase transitions, ^{13,14} transient band-structure 15,16 and band-gap renormalization, 17-19 and tunable valley polarization.^{5,20} While these phenomena are a manifestation of complex and diverse interaction mechanisms between electrons and lattice, a detailed understanding of the lattice dynamics and electron-phonon coupling in systems out of equilibrium remains elusive, and it keeps providing a strong stimulus for theoretical and experimental condensed-matter research. 5,13,16,21-23

Time- and angle-resolved photoemission spectroscopy (tr-ARPES) has led the way in the experimental investigation of the out-ofequilibrium carrier dynamic in TMDs, ²⁴ providing direct insight on the influence of electronphonon interactions on the carrier dynamics. 25 Information regarding the lattice and its nonequilibrium dynamics, however, can only be inferred indirectly from its effects on the electrons, as, e.g., transient changes of the Fermi level, electron binding energies, or quasiparticle linewidths. 15,16,26 Femtosecond electron diffuse scattering 27 (FEDS) probes the progressive change of phonon population as the dynamics of the coupled electron-phonon system evolves, 28 and it thus offer a more direct and detailed picture of the out-of-equilibrium dynamics of the lattice.²⁹ Recent FEDS measurements provide strong evidence that the thermalization of electronic and vibrational degrees of freedom in TMDs is characterized by striking anisotropies in the phonon population in reciprocal space. 30,31 These manifest themselves through the emergence of hot-spots in the FEDS intensity, which indicates local enhancement of the phonon population at selected high-symmetry points and directions in the Brillouin zone. 28,31–33,33,34

A quantitative understanding of these phenomena is challenging owing to the combined influence of valley degrees of freedom, lattice anharmonicities, and anisotropies of the electron-phonon interaction on the lattice dy-Despite providing valuable insight namics. into the carrier dynamics of two-dimensional and layered materials, 35-37 the concept of hot phonon – whereby the hot-carrier relaxation is assumed to be dominated by a few stronglycoupled phonon modes^{38–42} – is unsuitable for the description of these phenomena, since it inherently lacks a momentum-resolved description of the lattice dynamics. In the domain of first-principles calculations, conversely, the Boltzmann equation formalism 43-45 is emerging as a promising technique for investigating the influence of electron-phonon interactions on the nonequilibrium dynamics of electrons and phonons.

In this manuscript, the coupled nonequilibrium dynamics of electrons and phonons in monolayer MoS₂ is investigated from first principles based on the time-dependent Boltzmann equation. Many-body effects due to the electron-phonon and phonon-phonon interactions are explicitly accounted for within a new time-propagation algorithm, which enables the investigation of the nonequilibrium lattice dynamics with unprecedented resolution in reciprocal space. Inter-valley scattering processes in the relaxation path of excited carriers are found to influence thoroughly the lattice dynamics of monolayer MoS_2 , confining the phonon emission to the Γ and K high-symmetry points in the Brillouin zone. This mechanism is responsible for establishment of a non-thermal regime in the vibration of the crystalline lattice, which is characterized by a pronounced momentum anisotropy in the phonon population and is found to persist for several picoseconds. Overall, these findings suggest a new route to transiently control the phonon population, the electron-phonon coupling, and their nonequilibrium dynamics over timescales of several picoseconds.

At thermal equilibrium, the occupation of electronic and vibrational energy levels is given by the Fermi-Dirac and Bose-Einstein distribution functions, respectively:

$$f_{n\mathbf{k}}^{\text{FD}}(\mu, T) = [e^{(\varepsilon_{n\mathbf{k}} - \mu)/k_{\text{B}}T} + 1]^{-1}$$
 (1)
 $n_{\mathbf{q}\nu}^{\text{BE}}(T) = [e^{\hbar\omega_{\mathbf{q}\nu}/k_{\text{B}}T} - 1]^{-1}.$ (2)

$$n_{\mathbf{q}\nu}^{\text{BE}}(T) = [e^{\hbar\omega_{\mathbf{q}\nu}/k_{\text{B}}T} - 1]^{-1}.$$
 (2)

Here, $\varepsilon_{n\mathbf{k}}$ is the single-particle energy of a Bloch state, μ the chemical potential, $\hbar\omega_{\mathbf{q}\nu}$ the phonon energy, $k_{\rm B}$ the Boltzmann constant, and T the temperature. Out of equilibrium, either $f_{n\mathbf{k}}$ or $n_{\mathbf{q}\nu}$ differs from Eqs. (1) and (2), and the dynamics of the coupled electron-phonon system is driven by scattering processes between electrons and phonons. The time dependence of the distribution functions may be described within the Boltzmann equation formalism: 44-46

$$\partial_t f_{n\mathbf{k}}(t) = \Gamma_{n\mathbf{k}}^{\text{ep}}[f_{n\mathbf{k}}(t), n_{\mathbf{q}\nu}(t)]$$

$$\partial_t n_{\mathbf{q}\nu}(t) = \Gamma_{\mathbf{q}\nu}^{\text{pe}}[f_{n\mathbf{k}}(t), n_{\mathbf{q}\nu}(t)] + \Gamma_{\mathbf{q}\nu}^{\text{pp}}[n_{\mathbf{q}\nu}(t)]$$
(4)

where $\partial_t = \partial/\partial t$. The interplay of electronic and nuclear degrees of freedom is accounted for by the collision integrals for the electronphonon $(\Gamma_{n\mathbf{k}}^{\text{pp}})$, and phonon-electron $(\Gamma_{\mathbf{q}\nu}^{\text{pe}})$ interaction respectively, whereas $\Gamma_{\mathbf{q}\nu}^{pp}$ accounts for phonon-phonon scattering processes induced by lattice anharmonicities. Explicit expressions for the collision integrals are reported in the Supporting Information. Momentumresolution in the time-evolution of the electron distribution function is treated approximately by the introduction of a density-of-state approximation. 47,48 Radiative carrier recombination in MoS_2 occurs on time scales of the order of 1 ns^{49,50} or longer, ⁵¹ and it is hereby assumed to be inconsequential for the lattice dynamics. Electron-hole interactions are also neglected. Recent studies indicated that nonadiabatic effects⁵² may lead to a renormaliza-

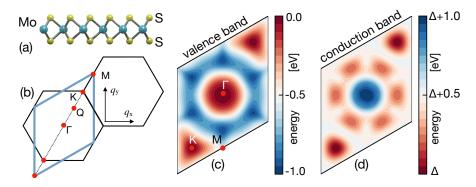


Figure 1: (a) Side view of the monolayer MoS_2 crystal structure. (b) Brillouin zone and high-symmetry points. The Γ -centered rhomboidal BZ is marked in blue. Energy dispersion of the valence (c) and conduction bands (d) in the BZ, as obtained from density-functional theory. Energies are relative to the valence band maximum, and $\Delta = 1.7$ eV is the energy of the Kohn-Sham band gap.

tion of the optical-phonon energy by up to 2 meV in doped MoS_2^{53-55} . These effects have been neglected here. To investigate the coupled nonequilibrium electron-phonon dynamics of monolayer MoS_2 , Eqs. (3) and (4) have been solved by time-stepping the time derivative for a total duration of 40 ps using a time step of 1 fs. Further details are found in the Supporting Information.

A side view of the monolayer MoS₂ crystal structure is shown in Fig. 1 (a), whereas its two-dimensional (2D) hexagonal Brillouin zone (BZ) is reported in Fig. 1 (b). In the following, the Γ -centered rhomboidal primitive cell in reciprocal space is considered (referred to below simply as BZ, and marked in blue in Fig. 1 (b)). For momenta in the BZ, the valence and conduction bands are illustrated in Figs. 1 (c) and (d), respectively, whereas the full band structure on a path is reported in Fig. 2 (a). Close to the gap, the valence band is characterized by a non-degenerate valley at Γ and a doublydegenerate valley at K, whereas the conduction band has a doubly-degenerate valley at K and a higher-energy sixfold-degenerate valley at Q. The co-existence of several quasi-degenerate valleys is shown below to play a key role in the nonequilibrium dynamics of the lattice.

In the following, I focus on a scenario in which the electron and lattice dynamics is triggered by the return to equilibrium of an electronic

excitation. The chosen initial state is representative of the excitation conditions that can be achieved in pump-probe experiments for monolayer MoS_2^{56} . At time t = 0, it is characterized by a density $n = 1 \cdot 10^{14} \text{ cm}^{-2}$ of electrons (holes) promoted to the conduction (valence) bands. Electronic occupations are given by a Fermi-Dirac distribution function $f_{n\mathbf{k}}(t=0) =$ $f_{n\mathbf{k}}^{\mathrm{FD}}(\mu_{\mathrm{e/h}}, T_{\mathrm{el}}^{0})$, with an effective electronic temperature $T_{\rm el}^0 = 2000$ K higher than the initial temperature of the lattice $T_{\rm ph}^0=100$ K. Other initial conditions are discussed in the Fig. S1 in the Supporting Information. The chemical potential of the electrons in the conduction band, $\mu_{\rm e}$, is determined through solution of the integral equation $n = \Omega_{\rm BZ}^{-1} \sum_{m}^{\rm cond.} \int d\mathbf{k} f_{m\mathbf{k}}^{0}(\mu_{\rm e}, T_{\rm el}^{0}),$ where $\Omega_{\rm BZ}$ is the area of the 2D Brillouin zone, and the sum extends over the conduction manifold. The hole chemical potential μ_h is determined analogously.

The carrier density n and the temperatures $T_{\rm el}^0$ and $T_{\rm ph}^0$ define the initial conditions for the propagation of Eqs. (3) and (4) in time. At thermal equilibrium ($T_{\rm el}^0 = T_{\rm ph}^0$), changes of $f_{n\bf k}$ due to the absorption and emission of phonons are exactly balanced, the right-hand side of Eq. (3) vanishes, and equilibrium is preserved ($\partial_t f_{n\bf k}(t) = 0$). The same applies to $n_{\bf q}_{\nu}$. Conversely, if $T_{\rm el}^0 > T_{\rm ph}^0$ electron-phonon scattering processes ensue to reestablish thermal equilibrium. The excess energy per unit cell of the ini-

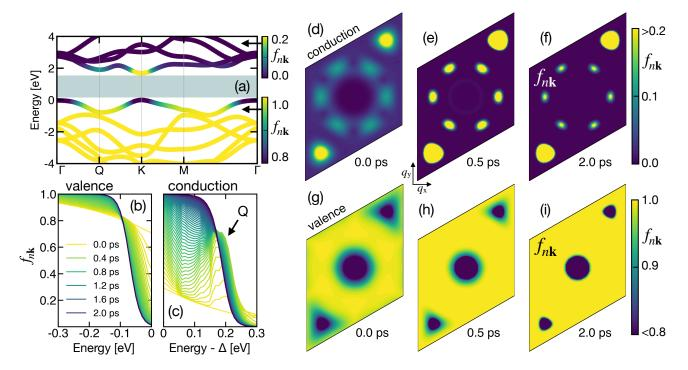


Figure 2: Nonequilibrium dynamics of electrons and holes in monolayer MoS₂. (a) DFT band structure and Fermi-Dirac occupations (superimposed as a color coding) for an initial excited electronic state $f_{n\mathbf{k}}(t=0)$. The band gap is shaded and different color scales are used for conduction and valence states, respectively. Time and energy dependence of the electron distribution function $f_{n\mathbf{k}}$ in the valence (b) and conduction (c) bands. The conduction-band energy is relative to the energy of the Kohn-Sham band gap ($\Delta = 1.7 \text{ eV}$). Time- and momentum-resolved electronic distribution function $f_{n\mathbf{k}}$ for crystal momenta in the full BZ for the conduction (d-f) and valence (g-i) bands at times t = 0, 0.5, and 2 ps.

tial electronic distribution can be estimated via $\Delta E_{\rm el} = \Omega_{\rm BZ}^{-1} \sum_n \int d\mathbf{k} \, \varepsilon_{n\mathbf{k}} [f_{n\mathbf{k}}^{\rm FD}(T_{\rm el}^0) - f_{n\mathbf{k}}^{\rm FD}(T_{\rm ph}^0)],$ which yields $\Delta E_{\rm el} = 35$ meV per unit cell for the conditions specified above.

In Fig. 2 (a), the electron distribution function $f_{n\mathbf{k}}(t=0)$ corresponding to the initial excited state is superimposed to the band dispersion of monolayer MoS₂. Bright regions in the conduction band reflect the initial population of excited electrons, whereas dark regions in the valence band indicate the hole population. The distribution function $f_{n\mathbf{k}}^0$ – further illustrated in the full BZ in Fig. 2 (d) and (g) for the conduction and valence bands, respectively – indicates that excited electrons (holes) primarily occupy states in the vicinity of the K and Q (K and Γ) high-symmetry points.

Figures 2 (b-c) report the electronic occupations $f_{n\mathbf{k}}$ in the valence and conduction bands, respectively, throughout the first 2 ps of the

dynamics. Since radiative recombination is neglected here, the total density of excited electrons and holes remains constant throughout the dynamics. The qualitative agreement between the temperature dependence of the Fermi-Dirac function (Fig. S4 of the Supporting Information) and the changes of the electronic occupations suggests an intuitive picture of the electron dynamics, whereby thermalization is achieved through a progressive lowering of the effective electronic temperature. It takes about 800 fs for excited holes in the valence band to thermalize with the lattice, whereas the electronic relaxation in the conduction band is completed within 2 ps. These time scales are in excellent agreement with recent femtosecond electron diffraction measurements on monolayer MoS_2 , ⁵⁷ which estimated to 1.7 ± 0.3 ps the timescale for electronic thermalization via electron-phonon scattering, whereas relaxation

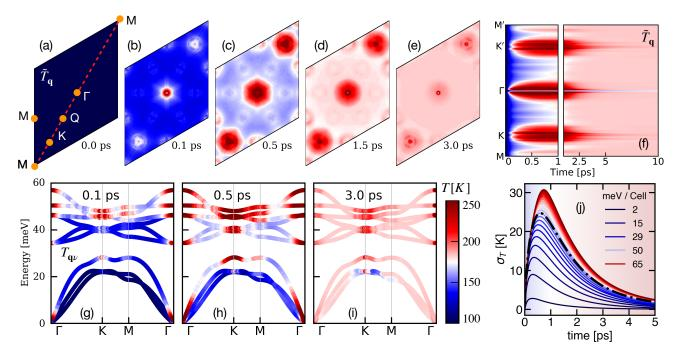


Figure 3: Nonequilibrium lattice dynamics of monolayer MoS_2 . (a) Momentum-resolved effective phonon temperature $\tilde{T}_{\bf q}$ (defined below Eq. (5)) at thermal equilibrium, and (b-e) at several time delays throughout the thermalization process. The same colors scale (color bar beside panel (i)) is used for panels (a-i). (f) Time dependence of the effective phonon temperature $\tilde{T}_{\bf q}\nu$ along the diagonal M-K-Γ-K-M path in the BZ (dashed line in panel (a)). (g-i) mode- and momentum-resolved effective phonon temperature $T_{\bf q}\nu$ (Eq. (5)) superimposed to the phonon dispersion of MoS_2 for $t=0.1,\ 0.5,\$ and $3.0\$ ps. (j) Standard deviation of the effective phonon temperature (Eq. (6)) for initial excitation energies $\Delta E_{\rm el}$ ranging between 2 and 65 meV per unit cell.

timescales of the order of 1 ps have been reported for few-layer samples. The different time scales for electron and hole relaxation can be ascribed to the co-existence of three quasi-degenerate valleys at Γ , K, and K' in the valence band, which in turn provide for a larger phase space for electron-phonon scattering. As electrons and lattice approach thermal equilibrium, $f_{n\mathbf{k}}$ converges towards a Fermi-Dirac function with final temperature $T_{\rm el}^{\rm fin}=180$ K (dark blue in Fig. 2 (b-c)).

Interestingly, while the distribution function $f_{n\mathbf{k}}$ remains monotonic in the valence band at each time step, revealing no traces of population inversion, a transient peak in the electronic occupations of the conduction band (arrow in Fig. 2 (c)) emerges over the first 300 fs at 200 meV above the conduction-band minimum, the energy of the six-fold degenerate Q pocket. This feature indicates that a bottleneck effect in the carrier relaxation may occur at Q, lead-

ing to a transient accumulation of hot carriers around the Q point, and it suggests that, similarly to WS_2 ,¹⁷ a regime of population inversion might be established in monolayer MoS_2 under suitable conditions of photo excitation.

A momentum-resolved view of the electron and hole dynamics is given by Figs. 2 (e-f) and (h-i), where values of $f_{n\mathbf{k}}$ in the full BZ are shown for the conduction and valence bands at selected time snapshots. Throughout the dynamics, excited electrons and holes remain localized in momentum space in the vicinity of the K and Γ high-symmetry points in the valence band, and around K and Q in the conduction band. As time evolves, the occupation of electronic states in the BZ – initially, more diffused owing to the higher electronic temperature – localizes further in the vicinity of high-symmetry points. This trend reflects a lowering of the electronic temperature as energy is transferred to the lattice and carriers scatter back to the Fermi energy.

Having discussed the dynamics of excited electrons and holes, I proceed next to discuss the out-of-equilibrium dynamics of the lattice. The effective *vibrational temperature* is defined as:

$$T_{\mathbf{q}\nu}(t) = \hbar\omega_{\mathbf{q}\nu} \{k_{\rm B} \ln[1 + n_{\mathbf{q}\nu}(t)]\}^{-1},$$
 (5)

and it is obtained by inverting the Bose-Einstein distribution, Eq. (2). At variance with $n_{\mathbf{q}\nu}$, $T_{\mathbf{q}\nu}$ becomes constant throughout the BZ at thermal equilibrium, and it is therefore better suited (but otherwise equivalent) to inspect the nonequilibrium dynamics of the lattice. Interpretation of $T_{\mathbf{q}\nu}$ as a thermodynamic temperature, however, is rigorously justified only at thermal equilibrium. Figures 3 (a-e) report the average vibrational temperature $\tilde{T}_{\mathbf{q}} = N_{\rm ph}^{-1} \sum_{\nu} T_{\mathbf{q}\nu}$ — with $N_{\rm ph} = 9$ being the number of phonon modes of monolayer MoS_2 — for crystal momenta within the first BZ and for selected time steps. The same color bar (shown beside panel (i)) is used for panels (a-i).

At t = 0 (Fig. 3 (a)), the lattice is at thermal equilibrium, as reflected by the constant vibrational temperature in the BZ $(T_{\mathbf{q}} =$ $T_{\rm ph}^0 = 100$ K). As the coupled electron-phonon dynamics begins (t > 0), the excited carriers in the valence and conduction bands relax back to Fermi level by transferring energy to the lattice through the emission of phonons. The influence of these processes on the phonon distribution function is accounted for by the phonon-electron collision integral $(\Gamma_{\mathbf{q}\nu}^{\mathrm{pe}})$ in Eq. (4), which leads to an increase of $n_{\mathbf{q}\nu}$ (and thus of $T_{\mathbf{q}\nu}$) as phonons with matching crystal momenta \mathbf{q} and index ν are emitted. After t = 100 fs (Fig. 3 (b)) the lattice has abandoned the initial thermalized state, as revealed by the emergence of hot-spots in the BZ characterized by a higher average vibrational temperature $T_{\mathbf{q}}$. In particular, an increase of the vibrational temperature is observed for momenta close to Γ and K, which in turn reflects an enhancement of the phonon population.

To understand the origin of these features, it should be noted that the emission of phonons – and, thus, the change of $T_{\mathbf{q}\nu}$ – is trig-

gered by electronic transitions within the valence and conduction bands, which are heavily constrained by energy and momentum conservation laws. For the excited electronic distribution of Fig. 2 (a), for instance, phononassisted transitions within the valence band primarily involve two types of processes: (i) intra-valley transitions, connecting initial and final electronic states both located close to the same high-symmetry point (Γ or K); (ii) intervalley transitions, with the initial and final electronic states located at Γ and K, respectively (or vice versa). Phonon-assisted transitions across the gap are forbidden by energy conservation. Due to momentum conservation, processes of type (i) result in the emission of longwavelength phonons ($\mathbf{q} \simeq 0$) with momenta close to Γ , whereas processes of type (ii) can only involve the emission phonons with momenta around K. A similar picture applies to transitions in the conduction band. Here, however, the presence of the Q valley also enables the emission of phonons around M and Q. A schematic illustration of the allowed inter- and intra-valley phonon-assisted transitions is provided in Fig. S2 of the Supporting Information. Umklapp processes are also included in this pictures, since transitions connecting different BZs can be folded back to the first BZ via translation by a reciprocal lattice vector. This picture enables us to attribute the anisotropic increase of vibrational temperature to the preferential emission of phonons at Γ and K, which is dictated by momentum selectivity in the electronic transitions.

This mechanism leads to a further enhancement of the temperature anisotropy in the BZ for t=500 fs (Fig. 3 (c)). Additionally, an increase in vibrational temperature is observed at the M point and, less pronouncedly, at Q, which arise from transitions involving the Q pocket in the conduction band. On longer time scales, phonon-phonon scattering – accounted for by the phonon-phonon collision integral ($\Gamma_{\mathbf{q}\nu}^{\mathrm{pp}}$) in Eq. (4) – counterbalances a non-thermal vibrational state by driving the lattice towards a thermalized regime (namely, $T_{\mathbf{q}\nu}$ = constant). This behaviour is manifested for t=1.5 and 3 ps (Figs. 3 (d-e)) by a progressive reduction

of the temperature anisotropy in the BZ.

The mode- and momentum-resolved vibrational temperature $T_{\mathbf{q}\nu}$ – superimposed to the phonon dispersion in Figs. 3 (g-i) for t = 0.1, 0.5, and 3 ps – may further change significantly for different phonon branches, since the contribution of each phonon to the relaxation process is dictated by its own electron-phonon coupling strength. 32,44 In particular, the stronger coupling of optical phonons makes them a more likely decay channel for the relaxation of excited carriers, as compared to other vibrations. This trend is reflected in Figs. 3 (g-h) by the higher vibrational temperature of these modes throughout the initial stages of the dynamics, suggesting that the electronic coupling to optical modes plays a primary role in the emergence of non-thermal state of the lattice.

A comprehensive picture of the formation and decay of a non-thermal vibrational state is provided in Fig. 3 (f), which illustrates the time evolution of the average vibrational temperature $\tilde{T}_{\mathbf{q}}$ for momenta along the M-K- Γ -K-M path in the BZ (dashed line in Fig. 3 (a)). The most striking manifestation of the nonequilibrium lattice dynamics are clearly visible up to t=5 ps, even though weaker anisotropies in the vibrational temperature persist for 10 ps or longer. The final temperature $(T_{\rm ph}^{\rm fin} \simeq 180~{\rm K})$ reached after $t \simeq 10$ ps coincides with the final electronic temperature $T_{\rm el}^{\rm fin}$, marking the recovery of thermal equilibrium between electrons and phonons. The time dependence of the temperature anisotropy of the lattice can be monitored by introducing the standard deviation σ_T :

$$\sigma_T = \Omega_{\rm BZ}^{-1} [\langle \tilde{T}_{\mathbf{q}}^2 \rangle_{\rm BZ} - \langle \tilde{T}_{\mathbf{q}} \rangle_{\rm BZ}^2]^{\frac{1}{2}}$$
 (6)

where $\langle \cdots \rangle_{\rm BZ}$ denotes the average over the Brillouin zone. In Fig. 3 (j), values of σ_T are reported for a concentration $n=1\cdot 10^{14}~{\rm cm}^{-2}$ of excited carriers and several initial excitation energies (in units of meV per unit cell). The dot-dashed line corresponds to the same initial condition of panels (a-i). σ_T vanishes at thermal equilibrium (t=0), and it increasingly differs from zero for larger deviation from a thermalized state. This trend leads to a well-defined maximum in σ_T at time delays between 200 and

900 fs, which marks the maximum anisotropy in the vibrational temperature. As more energy is provided to the initial electronic state, more time is required for the electrons to transfer their excess energy to the lattice via electron-phonon interactions, thus retarding the build-up of a nonequilibrium vibrational state. For all initial excited states, the return to a thermalized state takes place over timescales of the order of 5-10 ps.

Overall, this picture enables us to clearly identify different stages in the out-of-equilibrium dynamics of electrons and phonons in monolayer MoS₂: (i) following photo-excitation, electrons thermalize with the lattice within 2 ps via electron-phonon scattering; (ii) on time-scale shorter than 1 ps, momentum selectivity in the phonon-assisted electronic transitions induces a highly-anisotropic population of different phonons modes, driving the lattice into a non-thermal vibrational state; (iii) such non-thermal state persists for 5-10 picoseconds; (iv) thermal equilibrium is subsequently re-established by phonon-phonon scattering.

Remarkably, owing to the inherent mismatch between the characteristic time-scales for the electronic relaxation via phonon emission (< 2 ps) and lattice thermalization (> 5 ps), the mechanism that underpins the emergence of a non-thermal vibrational states is very robust upon changes of the initial excitation conditions (Fig. 3 (j)). This finding suggests that the transient enhancement of the phonon population at few selected high-symmetry points in the Brillouin zone could constitute a general characteristic of the nonequilibrium lattice dynamics of multi-valley semiconductors. Owing to the sensitivity of the electron-phonon interaction on the phonon population one can postulate that, under suitable condition of photo-excitation, the enhanced phonon population triggered by the nonequilibrium dynamics of the lattice may ultimately underpin transient changes of the electron-phonon interaction. If this scenario could be realized, it could reveal new directions towards the active control of many-body phenomena in quantum matter.

In conclusion, the coupled nonequilibrium dynamics of electrons and phonons in mono-

layer MoS₂ has been investigated by explicitly accounting for the effects of electron-phonon and phonon-phonon scattering within a firstprinciples time-dependent Boltzmann formal-Owing to phase-space constraints in inter- and intra-valley electronic transitions, the decay path of excited electrons and holes is dominated by the emission of phonons with momenta around few selected high-symmetry points in the Brillouin zone. Momentum selectivity in the phonon emission is found responsible for the emergence of a non-thermal vibrational state of the lattice which is characterized by a highly-anisotropic population of different phonon modes. Achieving control of non-thermal vibrational states and their lifetimes may provide unexplored opportunities to transiently tailor the electron-phonon coupling over time scales of several picoseconds.

Acknowledgement This project has been funded by the Deutsche Forschungsgemeinschaft (DFG) – Projektnummer 443988403.

Supporting Information Available: The Supporting Information is available free of charge.

Computational details; ^{59–65} first-principles expressions for the collision integrals; details on the numerical implementation of Eqs. (3) and (4); starting-point dependent of the nonequilibrium lattice dynamics; schematic illustration of the allowed inter- and intra-valley transitions for electron-phonon scattering.

References

- (1) Mak, K. F.; Lee, C.; Hone, J.; Shan, J.; Heinz, T. F. Atomically Thin MoS₂: A New Direct-Gap Semiconductor. *Phys. Rev. Lett.* **2010**, *105*, 136805.
- (2) Mueller, T.; Malic, E. Exciton physics and device application of two-dimensional transition metal dichalcogenide semiconductors. NPJ 2D Mater. Appl. 2018, 2, 29.
- (3) Zhou, B. T.; Taguchi, K.; Kawaguchi, Y.; Tanaka, Y.; Law, K. T. Spin-orbit coupling induced valley Hall effects in

- transition-metal dichalcogenides. Commun. Phys. **2019**, 2, 26.
- (4) Molina-Sánchez, A.; Sangalli, D.; Hummer, K.; Marini, A.; Wirtz, L. Effect of spin-orbit interaction on the optical spectra of single-layer, double-layer, and bulk MoS₂. *Phys. Rev. B* **2013**, *88*, 045412.
- (5) Beyer, H.; Rohde, G.; Grubišić Čabo, A.; Stange, A.; Jacobsen, T.; Bignardi, L.; Lizzit, D.; Lacovig, P.; Sanders, C. E.; Lizzit, S. et al. 80% Valley Polarization of Free Carriers in Singly Oriented Single-Layer WS₂ on Au(111). *Phys. Rev. Lett.* **2019**, 123, 236802.
- (6) Scuri, G.; Andersen, T. I.; Zhou, Y.; Wild, D. S.; Sung, J.; Gelly, R. J.; Bérubé, D.; Heo, H.; Shao, L.; Joe, A. Y. et al. Electrically Tunable Valley Dynamics in Twisted WSe₂/WSe₂ Bilayers. *Phys. Rev. Lett.* **2020**, *124*, 217403.
- (7) Kang, M.; Jung, S. W.; Shin, W. J.; Sohn, Y.; Ryu, S. H.; Kim, T. K.; Hoesch, M.; Kim, K. S. Holstein polaron in a valley-degenerate two-dimensional semiconductor. *Nat. Mater.* **2018**, *17*, 676–680.
- (8) Qiu, D. Y.; da Jornada, F. H.; Louie, S. G. Optical Spectrum of MoS₂: Many-Body Effects and Diversity of Exciton States. Phys. Rev. Lett. 2013, 111, 216805.
- (9) Briggs, N.; Bersch, B.; Wang, Y.; Jiang, J.; Koch, R. J.; Nayir, N.; Wang, K.; Kolmer, M.; Ko, W.; De La Fuente Duran, A. et al. Atomically thin half-van der Waals metals enabled by confinement heteroepitaxy. *Nat. Mater.* **2020**, *19*, 637–643.
- (10) Kang, K.; Xie, S.; Huang, L.; Han, Y.; Huang, P. Y.; Mak, K. F.; Kim, C.-J.; Muller, D.; Park, J. High-mobility three-atom-thick semiconducting films with wafer-scale homogeneity. *Nature* **2015**, 520, 656–660.

- (11) Cuadra, J.; Baranov, D. G.; Wersäll, M.; Verre, R.; Antosiewicz, T. J.; Shegai, T. Observation of Tunable Charged Exciton Polaritons in Hybrid Monolayer WS₂ Plasmonic Nanoantenna System. Nano Lett. 2018, 18, 1777-1785.
- (12) Basov, D. N.; Averitt, R. D.; Hsieh, D. Towards properties on demand in quantum materials. *Nat. Mater.* **2017**, *16*, 1077–1088.
- (13) Hellmann, S.; Beye, M.; Sohrt, C.; Rohwer, T.; Sorgenfrei, F.; Redlin, H.; Kalläne, M.; Marczynski-Bühlow, M.; Hennies, F.; Bauer, M. et al. Ultrafast Melting of a Charge-Density Wave in the Mott Insulator 1T—TaS₂. Phys. Rev. Lett. **2010**, 105, 187401.
- (14) Hellmann, S.; Rohwer, T.; Kalläne, M.; Hanff, K.; Sohrt, C.; Stange, A.; Carr, A.; Murnane, M.; Kapteyn, H.; Kipp, L. et al. Time-domain classification of charge-density-wave insulators. *Nat. Commun.* **2012**, *3*, 1069.
- (15) Yang, L. X.; Rohde, G.; Rohwer, T.; Stange, A.; Hanff, K.; Sohrt, C.; Rettig, L.; Cortés, R.; Chen, F.; Feng, D. L. et al. Ultrafast Modulation of the Chemical Potential in BaFe₂As₂ by Coherent Phonons. *Phys. Rev. Lett.* **2014**, *112*, 207001.
- (16) Hein, P.; Jauernik, S.; Erk, H.; Yang, L.; Qi, Y.; Sun, Y.; Felser, C.; Bauer, M. Mode-resolved reciprocal space mapping of electron-phonon interaction in the Weyl semimetal candidate Td-WTe₂. Nat. Commun. 2020, 11, 2613.
- (17) Chernikov, A.; Ruppert, C.; Hill, H. M.; Rigosi, A. F.; Heinz, T. F. Population inversion and giant bandgap renormalization in atomically thin WS₂ layers. *Nat. Photon.* **2015**, *9*, 466–470.
- (18) Pogna, E. A. A.; Marsili, M.; De Fazio, D.; Dal Conte, S.; Manzoni, C.; Sangalli, D.; Yoon, D.; Lombardo, A.; Ferrari, A. C.;

- Marini, A. et al. Photo-Induced Bandgap Renormalization Governs the Ultrafast Response of Single-Layer MoS₂. *ACS Nano* **2016**, *10*, 1182–1188.
- (19) Wood, R. E.; Lloyd, L. T.; Mujid, F.; Wang, L.; Allodi, M. A.; Gao, H.; Mazuski, R.; Ting, P.-C.; Xie, S.; Park, J. et al. Evidence for the Dominance of Carrier-Induced Band Gap Renormalization over Biexciton Formation in Cryogenic Ultrafast Experiments on MoS₂ Monolayers. J. Phys. Chem. Lett. **2020**, 11, 2658–2666.
- (20) Berghäuser, G.; Bernal-Villamil, I.; Schmidt, R.; Schneider, R.; Niehues, I.; Erhart, P.; Michaelis de Vasconcellos, S.; Bratschitsch, R.; Knorr, A.; Malic, E. Inverted valley polarization in optically excited transition metal dichalcogenides. Nat. Commun. 2018, 9, 971.
- (21) De Giovannini, U.; Hübener, H.; Rubio, A. Monitoring Electron-Photon Dressing in WSe₂. Nano Lett. **2016**, 16, 7993–7998.
- (22) Selig, M.; Katsch, F.; Schmidt, R.; Michaelis de Vasconcellos, S.; Bratschitsch, R.; Malic, E.; Knorr, A. Ultrafast dynamics in monolayer transition metal dichalcogenides: Interplay of dark excitons, phonons, and intervalley exchange. *Phys. Rev. Res.* **2019**, *1*, 022007.
- (23) Molina-Sánchez, A.; Sangalli, D.; Wirtz, L.; Marini, A. Ab Initio Calculations of Ultrashort Carrier Dynamics in Two-Dimensional Materials: Valley Depolarization in Single-Layer WSe₂. Nano Lett. 2017, 17, 4549–4555.
- (24) Grubišić Čabo, A.; Miwa, J. A.; Grønborg, S. S.; Riley, J. M.; Johannsen, J. C.; Cacho, C.; Alexander, O.; Chapman, R. T.; Springate, E.; Grioni, M. et al. Observation of Ultrafast Free Carrier Dynamics in Single Layer MoS₂. Nano Lett. **2015**, 15, 5883–5887.
- (25) Chen, Z.; Sjakste, J.; Dong, J.; Taleb-Ibrahimi, A.; Rueff, J.-P.; Shukla, A.;

- Peretti, J.; Papalazarou, E.; Marsi, M.; Perfetti, L. Ultrafast dynamics of hot carriers in a quasi–two-dimensional electron gas on InSe. *Proc. Natl. Acad. Sci.* **2020**, 117, 21962–21967.
- (26) Schmitt, F.; Kirchmann, P. S.; Bovensiepen, U.; Moore, R. G.; Rettig, L.; Krenz, M.; Chu, J.-H.; Ru, N.; Perfetti, L.; Lu, D. H. et al. Transient Electronic Structure and Melting of a Charge Density Wave in TbTe₃. **2008**, *321*, 1649–1652.
- (27) Sciaini, G.; Miller, R. J. D. Femtosecond electron diffraction: heralding the era of atomically resolved dynamics. *Rep. Prog. Phys.* **2011**, 74, 096101.
- (28) René de Cotret, L. P.; Pöhls, J.-H.; Stern, M. J.; Otto, M. R.; Sutton, M.; Siwick, B. J. Time- and momentum-resolved phonon population dynamics with ultrafast electron diffuse scattering. *Phys. Rev. B* **2019**, *100*, 214115.
- (29) Siwick, B. J.; Dwyer, J. R.; Jordan, R. E.; Miller, R. J. D. An Atomic-Level View of Melting Using Femtosecond Electron Diffraction. *Science* **2003**, *302*, 1382–1385.
- (30) Waldecker, L.; Bertoni, R.; Hübener, H.; Brumme, T.; Vasileiadis, T.; Zahn, D.; Rubio, A.; Ernstorfer, R. Momentum-Resolved View of Electron-Phonon Coupling in Multilayer WSe₂. *Phys. Rev. Lett.* **2017**, *119*, 036803.
- (31) Otto, M. R.; Pöhls, J.-H.; de Cotret, L. P. R.; Stern, M. J.; Sutton, M.; Siwick, B. J. Mechanisms of electron-phonon coupling unraveled in momentum and time: The case of soft-phonons in TiSe₂. arXiv 2020, 1912.03559.
- (32) Stern, M. J.; René de Cotret, L. P.; Otto, M. R.; Chatelain, R. P.; Boisvert, J.-P.; Sutton, M.; Siwick, B. J. Mapping momentum-dependent electron-phonon coupling and nonequilibrium phonon dynamics with ultrafast electron diffuse

- scattering. *Phys. Rev. B* **2018**, *97*, 165416.
- (33) Seiler, H.; Zahn, D.; Zacharias, M.; Hildebrandt, P.; Vasileiadis, T.; Windsor, Y. W.; Qi, Y.; Carbogno, C.; Draxl, C.; Caruso, F. et al. Accessing the anisotropic non-thermal phonon populations in black phosphorus. arXiv 2020, 2006.12873.
- (34) Krishnamoorthy, A.; Lin, M.-F.; Zhang, X.; Weninger, C.; Ma, R.; Britz, A.; Tiwary, C. S.; Kochat, V.; Apte, A.; Yang, J. et al. Optical Control of Non-Equilibrium Phonon Dynamics. *Nano Lett.* **2019**, *19*, 4981–4989.
- (35) Johannsen, J. C.; Ulstrup, S.; Cilento, F.; Crepaldi, A.; Zacchigna, M.; Cacho, C.; Turcu, I. C. E.; Springate, E.; Fromm, F.; Raidel, C. et al. Direct View of Hot Carrier Dynamics in Graphene. *Phys. Rev. Lett.* **2013**, *111*, 027403.
- (36) Stange, A.; Sohrt, C.; Yang, L. X.; Rohde, G.; Janssen, K.; Hein, P.; Oloff, L.-P.; Hanff, K.; Rossnagel, K.; Bauer, M. Hot electron cooling in graphite: Supercollision versus hot phonon decay. *Phys. Rev. B* **2015**, *92*, 184303.
- (37) Waldecker, L.; Bertoni, R.; Ernstorfer, R.; Vorberger, J. Electron-Phonon Coupling and Energy Flow in a Simple Metal beyond the Two-Temperature Approximation. *Phys. Rev. X* **2016**, *6*, 021003.
- (38) Allen, P. B. Theory of thermal relaxation of electrons in metals. *Phys. Rev. Lett.* **1987**, *59*, 1460–1463.
- (39) Lin, Z.; Zhigilei, L. V.; Celli, V. Electron-phonon coupling and electron heat capacity of metals under conditions of strong electron-phonon nonequilibrium. *Phys. Rev. B* **2008**, *77*, 075133.
- (40) Novko, D.; Tremblay, J. C.; Alducin, M.; Juaristi, J. I. Ultrafast Transient Dynamics of Adsorbates on Surfaces Deciphered:

- The Case of CO on Cu(100). *Phys. Rev. Lett.* **2019**, *122*, 016806.
- (41) Novko, D.; Caruso, F.; Draxl, C.; Cappelluti, E. Ultrafast Hot Phonon Dynamics in MgB₂ Driven by Anisotropic Electron-Phonon Coupling. *Phys. Rev. Lett.* 2020, 124, 077001.
- (42) Caruso, F.; Novko, D.; Draxl, C. Photoemission signatures of nonequilibrium carrier dynamics from first principles. *Phys. Rev. B* **2020**, *101*, 035128.
- (43) Ziman, J. M. Electrons and phonons: the theory of transport phenomena in solids; Clarendon Press: Oxford, 1960.
- (44) Sadasivam, S.; Chan, M. K. Y.; Darancet, P. Theory of Thermal Relaxation of Electrons in Semiconductors. *Phys. Rev. Lett.* **2017**, *119*, 136602.
- (45) Jhalani, V. A.; Zhou, J.-J.; Bernardi, M. Ultrafast Hot Carrier Dynamics in GaN and Its Impact on the Efficiency Droop. Nano Lett. 2017, 17, 5012–5019.
- (46) Haug, H.; Jauho, A. Quantum Kinetics in Transport and Optics of Semiconductors; Springer Series in Solid-State Sciences; Springer Berlin Heidelberg, 2007.
- (47) Zhukov, V. P.; Tyuterev, V. G.; Chulkov, E. V.; Echenique, P. M. Electron-phonon relaxation and excited electron distribution in gallium nitride. *J. Appl. Phys.* **2016**, *120*, 085708.
- (48) Sjakste, J.; Tanimura, K.; Barbarino, G.; Perfetti, L.; Vast, N. Hot electron relaxation dynamics in semiconductors: assessing the strength of the electron–phonon coupling from the theoretical and experimental viewpoints. J. Phys. Conden. Matter 2018, 30, 353001.
- (49) Amani, M.; Lien, D.-H.; Kiriya, D.; Xiao, J.; Azcatl, A.; Noh, J.; Madhvapathy, S. R.; Addou, R.; KC, S.; Dubey, M. et al. Near-unity photoluminescence quantum yield in MoS₂. Science 2015, 350, 1065–1068.

- (50) Yu, Y.; Yu, Y.; Xu, C.; Barrette, A.; Gundogdu, K.; Cao, L. Fundamental limits of exciton-exciton annihilation for light emission in transition metal dichalcogenide monolayers. *Phys. Rev. B* **2016**, *93*, 201111.
- (51) Bataller, A. W.; Younts, R. A.; Rustagi, A.; Yu, Y.; Ardekani, H.; Kemper, A.; Cao, L.; Gundogdu, K. Dense Electron-Hole Plasma Formation and Ultralong Charge Lifetime in Monolayer MoS₂ via Material Tuning. Nano Lett. 2019, 19, 1104-1111.
- (52) Caruso, F.; Hoesch, M.; Achatz, P.; Serrano, J.; Krisch, M.; Bustarret, E.; Giustino, F. Nonadiabatic Kohn Anomaly in Heavily Boron-Doped Diamond. *Phys. Rev. Lett.* **2017**, *119*, 017001.
- (53) Sohier, T.; Ponomarev, E.; Gibertini, M.; Berger, H.; Marzari, N.; Ubrig, N.; Morpurgo, A. F. Enhanced Electron-Phonon Interaction in Multivalley Materials. *Phys. Rev. X* **2019**, *9*, 031019.
- (54) Novko, D. Broken adiabaticity induced by Lifshitz transition in MoS2 and WS2 single layers. *Communications Physics* **2020**, 3, 30.
- (55) Garcia-Goiricelaya, P.; Lafuente-Bartolome, J.; Gurtubay, I. G.; Eiguren, A. Emergence of large nonadiabatic effects induced by the electron-phonon interaction on the complex vibrational quasiparticle spectrum of doped monolayer MoS₂. Phys. Rev. B **2020**, 101, 054304.
- (56) Seo, M.; Yamaguchi, H.; Mohite, A. D.; Boubanga-Tombet, S.; Blancon, J.-C.; Najmaei, S.; Ajayan, P. M.; Lou, J.; Taylor, A. J.; Prasankumar, R. P. Ultrafast Optical Microscopy of Single Monolayer Molybdenum Disulfide Flakes. Scientific Reports 2016, 6, 21601.
- (57) Mannebach, E. M.; Li, R.; Duerloo, K.-A.; Nyby, C.; Zalden, P.; Vecchione, T.;

- Ernst, F.; Reid, A. H.; Chase, T.; Shen, X. et al. Dynamic Structural Response and Deformations of Monolayer MoS_2 Visualized by Femtosecond Electron Diffraction. *Nano Lett.* **2015**, *15*, 6889–6895.
- (58) Nie, Z.; Long, R.; Sun, L.; Huang, C.-C.; Zhang, J.; Xiong, Q.; Hewak, D. W.; Shen, Z.; Prezhdo, O. V.; Loh, Z.-H. Ultrafast Carrier Thermalization and Cooling Dynamics in Few-Layer MoS₂. ACS Nano 2014, 8, 10931–10940.
- (59) Hohenberg, P.; Kohn, W. Inhomogeneous Electron Gas. *Phys. Rev.* **1964**, *136*, B864–B871.
- (60) Kohn, W.; Sham, L. J. Self-Consistent Equations Including Exchange and Correlation Effects. *Phys. Rev.* **1965**, *140*, A1133–A1138.
- (61) Giannozzi, P.; Andreussi, O.; Brumme, T.; Bunau, O.; Nardelli, M. B.; Calandra, M.; Car, R.; Cavazzoni, C.; Ceresoli, D.; Cococcioni, M. et al. Advanced capabilities for materials modelling with Quantum ESPRESSO. J. Phys. Condens. Matter 2017, 29, 465901.
- (62) Perdew, J. P.; Wang, Y. Accurate and simple analytic representation of the electrongas correlation energy. *Phys. Rev. B* **1992**, 45, 13244–13249.
- (63) Pizzi, G.; Vitale, V.; Arita, R.; Blügel, S.; Freimuth, F.; Géranton, G.; Gibertini, M.; Gresch, D.; Johnson, C.; Koretsune, T. et al. Wannier90 as a community code: new features and applications. *J. Phys. Condens. Matter.* **2020**, *32*, 165902.
- (64) Poncé, S.; Margine, E.; Verdi, C.; Giustino, F. EPW: Electron-phonon coupling, transport and superconducting properties using maximally localized Wannier functions. *Comp. Phys. Commun.* **2016**, *209*, 116–133.
- (65) Li, W.; Carrete, J.; Katcho, N. A.; Mingo, N. ShengBTE: a solver of the Boltzmann transport equation for

phonons. Comp. Phys. Commun. **2014**, 185, 1747–1758.